PCCP

ROYAL SOCIETY OF CHEMISTRY

PAPER

View Article Online
View Journal | View Issue

Check for updates

Cite this: *Phys. Chem. Chem. Phys.*, 2021, **23**, 5431

Structure and electronic bandgap tunability of *m*-plane GaN multilayers†

Xueru Cai, Yiming Ma, Jinlong Ma, Dongwei Xu * and Xiaobing Luo

Received 24th November 2020,
Accepted 20th January 2021

DOI: 10.1039/d0cp06093c

rsc.li/pccp

Two-dimensional (2D) gallium nitride (GaN) has attracted a lot of attention due to its promising applications in photoelectric nano-devices. Most previous research studies have focused on polar *c*-plane 2D structures. Here, by employing first principles calculations, we systematically investigate the structural and electronic properties of non-polar *m*-plane GaN with different numbers of atomic layers. The results show a layer-dependent structure transition and electronic band variation for *m*-plane GaN. It is found that the monolayer keeps a planar hexagonal structure due to sp^2 hybridization, whereas the multilayers are formed by stacking of buckled hexagonal monolayers with unsaturated coordination number at the surface sublayer and bulk-like inner layers. These discrepancies in the structure further induce an indirect to direct transition of the band gap type when the layer number reaches twelve. By carefully examining the relationship between the structure and electronic bandgap, we find that the indirect bandgap comes from the unsaturated surface with a planar like structure. On surface modification, saturation of the surface dangling bonds results in an indirect to direct band gap transition.

1. Introduction

In contrast to conventional 2D materials such as graphene, MoS_2 and β-tellurene,[1–3] for which interlayer interactions are dominated by van der Waals forces, 2D non-layered materials, in which interlayer atoms are connected by strong chemical bonds, are another important category in 2D materials. Caused by the breaking of bonds in the out-of-plane direction when the material's dimensions are reduced from 3D to 2D, the highly exposed dangling bonds on the surfaces of non-layered 2D materials endow these surfaces with interesting electronic, magnetic, optical and catalytic properties.[5] Moreover, these dangling bonds naturally provide lots of active sites for chemical modifications such as atom adsorption and incorporation, further increasing the possibility to modulate surface properties by surface engineering.[6] For example, it has been proved experimentally that hydrogenation and fluorination can largely tune the electronic and optical properties of graphene, promoting the application potential of these materials.[7–10]

Gallium nitride (GaN), a typical non-layered material which is widely applied in the fabrication of light-emitting diodes (LEDs), has been extensively investigated for its excellent electronic and optical properties.[11] Motivated by the exploration of 2D materials and the unique properties they have manifested, 2D GaN has also drawn much research attention. Most of the researchers have focused on the polar *c*-plane of GaN. Colin L. Freeman *et al.*[12] firstly modelled the polar *c*-plane. They proposed a graphite-like GaN film structure and demonstrated that the charge transfer on the surface is the key to stabilize the structure. D. Xu *et al.*[13] further studied the effect of stacking sequence on the stability of the GaN multilayers, indicating that the structure with Ga(N) atoms on top of N(Ga) atoms was the most stable form. Following the work of Freeman and Xu, A. V. Kolobov *et al.* argued that GaN is unstable in the graphitic phase and proposed an 8|4 Haeckelite ring phase with stability verified by phonon calculation.[14] The study indicated that the covalently bonded GaN would not form stable structures by stacking 2–4 flat graphene-like monolayers. It is well known that the *c*-plane of GaN is a polar plane with cations and anions lying in different planes. According to Tasker's theory,[15] this kind of type III structure is intrinsically unstable because of the divergence of the surface energy. When truncated from different crystal planes, there could exist four typical forms of GaN thin films: polar *c*-plane along (0001), nonpolar *m*-plane along $(10\bar{1}0)$, nonpolar *a*-plane along $(1\bar{2}10)$ and semipolar *r*-plane along $(11\bar{2}2)$. Different from the polar *c*-plane, Ga and N atoms locate in the same plane for the nonpolar *m*-plane. This indicates that the multilayer *m*-plane GaN may be stable. While lots of effort has been put into the structural and electronic properties of the *m*-plane surface,[16–18] the properties of few-layer GaN along the *m*-plane remain unexplored.

State Key Laboratory of Coal Combustion, School of Energy and Power Engineering, Huazhong University of Science and Technology, Wuhan, Hubei 430074, China. E-mail: dwxu@hust.edu.cn

† Electronic supplementary information (ESI) available. See DOI: 10.1039/d0cp06093c

One reason for the wide applications of GaN is its wide direct bandgap. With the demand of miniaturization and integration, the nanoscale materials have been paid great attention. However, when the dimension is reduced to 2D for GaN, the bandgap turns out to be indirect.[19,20] From the aspect of application, we are interested in three points: (1) how the bandgap changes with the atomic layer number, (2) how to tune the bandgap from indirect to direct and (3) how to control the width of the bandgap.

In this work, by carrying out density functional theory calculations, we investigate the structure and electronic properties of the *m*-plane GaN thin film with the number of atomic layers changing from monolayer (ML) to fourteen layers systematically. The structural stability of the predicted *m*-plane GaN is verified by phonon calculations and cohesive energy. We find a coordination number dependent variation of bond length and bond angle, and a layer-dependent band alignment in *m*-plane GaN. The Ga/N atom with coordination number equal to three has a stronger bond strength, leading to more distorted tetrahedral units. With the increase of layer number, we find an indirect to direct shift for bandgap. In addition, we disclose that surface modification by hydrogenation and fluorination can significantly enlarge the bandgap and turn an indirect gap into a direct one.

2. Computational methods

Density functional theory calculations are performed using the Vienna ab intio Simulation Package (VASP).[21,22] The projector-augmented-wave (PAW) potentials are used for Ga and N where the 3d electrons of Ga are described as valence.[23] The generalized gradient approximation (GGA) in the form of Perdew, Burke and Ernzerhof (PBE) is used for the exchange correlation functional. The hybrid Heyd–Scuseria–Ernzerhof (HSE06) functional is also introduced to verify the bandgap tendency predicted from PBE calculation. DFT-D3 of Grimme method is applied to describe the vdW interaction.[24] A vacuum distance larger than 15 Å is set to prevent the interaction of neighbouring images. The cut-off energy for the plane wave basis is 520 eV for pristine and hydrogenated GaN and 900 eV for fluorinated one. The convergence criteria for energy and force are set as 10^{-6} eV and 10^{-2} eV Å^{-1} respectively. A $15 \times 9 \times 1$ Gamma-centered *k* mesh is used to sample the Brillouin-zone. Phonon dispersion is calculated to verify the stability of structures by using the phonopy package.[25] The force constants for the dynamical matrix are computed with a $6 \times 4 \times 1$ supercell, based on the density functional perturbation theory (DFPT) as implemented in VASP. The bond order is calculated with DDEC6[26] methods as implemented in Chargemol.[27]

3. Results and discussion

3.1 Structure of *m*-plane GaN

As mentioned above, multilayer *m*-plane GaN is obtained by truncating the bulk along the $(10\bar{1}0)$ plane. The schematic diagram of the pristine monolayer is shown in Fig. 1(a).

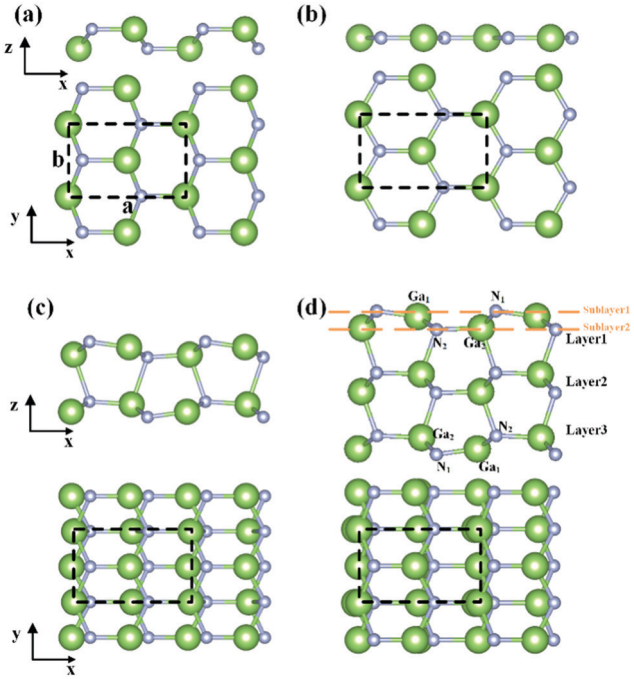

Fig. 1 Side and top views of (a) the pristine *m*-plane GaN monolayer, (b) optimized monolayer *m*-plane GaN, (c) optimized bilayer *m*-plane GaN, (d) optimized trilayer *m*-plane GaN (grey: N atom, green: Ga atom). Unit cells are outlined by dotted rectangles. The figures are drawn using VESTA.[4]

The buckled structure forms an irregular hexagon. Different from the polar *c*-plane in which the N and Ga atoms locate in different layers separately,[28] the truncated pristine *m*-plane GaN forms a nonpolar structure in which N and Ga equally arrange in each sublayer of the monolayer. We call it the buckled hexagonal structure for simplicity. Such a discrepancy between *m*-plane GaN and *c*-plane GaN would further induce a series of differences in the structures and electronic properties as will be discussed later.

The optimized *m*-plane GaN monolayer is shown in Fig. 1(b). Compared with the pristine case, it is interesting that the structure evolves into a planar regular hexagonal structure, the same as the optimized *c*-plane GaN monolayer. The bond length of the monolayer is 1.85 Å with a bond angle of 120°, in good agreement with the former studies on monolayer hexagonal GaN.[13,19] We also optimize the truncated *a*-plane GaN monolayer and get the same hexagonal structure (as illustrated in Fig. S1 in ESI†). These results indicate that no matter what the initial structure is, the most stable monolayer structure is the hexagonal one. Moving from bulk GaN to the monolayer structure, the number of bonds between Ga and N reduces from 4 to 3 and the sp^3 hybridization changes to sp^2 hybridization, following the change of the structure from a tetrahedron to a planar hexagon.

A systematic study of the atomic structure as a function of atomic layer number from 1 to 14 is performed. The optimized multilayer *m*-plane GaN shows a distinctly different structure from the optimized monolayer *m*-plane and multilayer *c*-plane GaN. For the structural similarity of multilayers, we take trilayer

m-plane GaN as a representative for the sake of conciseness. As shown in Fig. 1(d), trilayer *m*-plane GaN is formed by stacking three buckled hexagonal monolayers. This is totally different from the *c*-plane GaN multilayers which are stacked with planar hexagonal structures or the 8|4 heackelite *c*-plane which is comprised of alternating octagonal and square rings.[13,14,19] The non-layered structure implies that the hybridization is no longer sp^2. The Ga/N atom in the middle layer (denoted as layer2) has four coordination numbers (n_c) as in the bulk. Two distinct types of Ga/N atoms with different n_c exist on the surface layer (denoted as layer1 and layer3): the outer Ga and N atoms (denoted as Ga_1 and N_1) in sublayer1 with $n_c = 3$ and the inner Ga and N atoms (denoted as Ga_2 and N_2) in sublayer 2 with $n_c = 4$. Such distinctions of coordination number further induce discrepancies in bond length and bond angle, as listed in Table 1. For the outer layers, there are four types of bond length. The shortest one is the bond between Ga_1 and N_1 each with coordination number three and the longest one is the bond between Ga_2 and N_2 each with coordination number four. Moreover, the bond angle within the outer layer deviates from the bulk more significantly than the central layer, which tends to adopt the planar 3-coordinated hexagonal structure. These structural properties of *m*-plane GaN multilayers are consistent with the distortion of surface layers in bulk GaN with *m*-plane surfaces.[17,18,29]

From the results and discussion above, the 2D *m*-plane could be classified into three types: (1) optimized monolayer with all the Ga/N atoms 3-coordinated, (2) bilayer *m*-plane consisting of only two surface layers with both 3- and 4-coordination, and (3) multilayer *m*-plane with both inner bulk-like layers and surface layers. The structural stability is verified by the phonon spectrum and cohesive energy as shown in the ESI† (see Fig. S2).

3.2 Electronic band structures of *m*-plane GaN

As we all know, PBE calculations usually underestimate material bandgaps compared with the experiments. The HSE06 hybrid functional has been confirmed to be a good approach to accurately calculate the electronic band while it is quite time consuming. For this reason, we only calculate the HSE band from monolayer to five layers. Apart from the difference in the specific values of band gaps, the orbital projected electronic structure and the bandgap variation trend with layer numbers that will be discussed below are consistent with the PBE calculations as shown in Supplementary Materials (see Fig. S3, ESI†). In the following part, we focus on the results from PBE calculations.

3.2.1 Band structure of monolayer GaN. The band structures of different layers are calculated to investigate the electronic properties of *m*-plane GaN. The electronic bands are processed with the VASPKIT code.[30] The orbital projected band structure of monolayer GaN is shown in Fig. 2(a) and (b), in comparison with the bulk GaN band structure in Fig. 2(d) and (e). The band gap changes from direct in bulk to indirect in the monolayer. A remarkable shift of the valence-band maximum (VBM) is observed. For the monolayer, the VBM locates between Γ and Y and the conduction band minimum (CBM) locates at Γ, forming a 2.18 eV indirect bandgap, while the bulk has a direct bandgap of 1.82 eV. The CBM is at the Γ point and contributed by the Ga atoms. The main contribution to the VBM is the p-orbital of the N atoms for both monolayer and bulk as shown by the red circles in Fig. 2(a) and (d). The hybridized p orbitals contribute equally at the Γ point for the bulk. However, there is a large contribution of the p_z orbital of N atoms in the Γ to Y direction resulting in the indirect bandgap of the monolayer. From the charge distribution shown in Fig. 2(f), we can see that the Ga and N atoms are sp^3 hybridized in the bulk and form a tetrahedral structure. For the monolayer GaN, due to the missing bonds between Ga and N, the hybridization changes to sp^2 and a planar hexagonal structure is formed as shown in Fig. 2(c). These results are consistent with previous research about the optimized monolayer *c*-plane GaN which is also the planar hexagonal structure.[20]

3.2.2 Band structure of the bilayer *m*-plane structure. For the bilayer structure, there are two surface layers with outer

Table 1 Information of lattice constants, bandgap, bond angle, bond length and bond order

Layer	Lattice constant *b* (Å)	Lattice constant *a* (Å)	Band gap (eV)	Type	ΘN_2–Ga_1–N_2 (°)	ΘN_1–Ga_2–N_1 (°)	Bond length N_1–Ga_1 (Å)	Bond order of N_1–Ga_1
1L	3.2054	5.5519	2.184	Indirect	120.00	119.9991	1.8506	0.9945
2L	3.2512	5.3405	1.66	Indirect	117.907	119.301	1.8402	0.9880
3L	3.2381	5.2654	1.455	Indirect	115.0675	116.657	1.8281	1.0226
4L	3.2286	5.2488	1.457	Indirect	114.3965	115.9403	1.8258	1.0284
5L	3.2215	5.2406	1.49	Indirect	114.1438	115.6511	1.8251	1.0292
6L	3.2172	5.236	1.522	Indirect	113.9221	115.3759	1.8248	1.0292
7L	3.2145	5.2336	1.548	Indirect	113.8276	115.2565	1.8245	1.0294
8L	3.2127	5.2319	1.57	Indirect	113.7772	115.2013	1.8244	1.0290
9L	3.2100	5.2295	1.585	Indirect	113.6896	115.0811	1.8242	1.0290
10L	3.2084	5.2281	1.599	Indirect	113.6332	115.0179	1.8241	1.0287
11L	3.2079	5.2275	1.612	Indirect	113.6078	115.0001	1.8240	1.0290
12L	3.2068	5.2266	1.618	Direct	113.5970	114.9548	1.8239	1.0286
13L	3.2058	5.2258	1.618	Direct	113.5535	114.9188	1.8238	1.0293
14L	3.2041	5.2243	1.619	Direct	113.4940	114.8410	1.8237	1.0281
Bulk	3.1999	5.2186	1.818	Direct	109.6762	109.6762	1.9571	0.6779
H(3L)	3.1979	5.2349	2.952	Direct	107.9924	109.2278	1.9937	0.6592
F(3L)	3.2238	5.3270	2.076	Direct	108.8311	110.6556	2.0168	0.5511

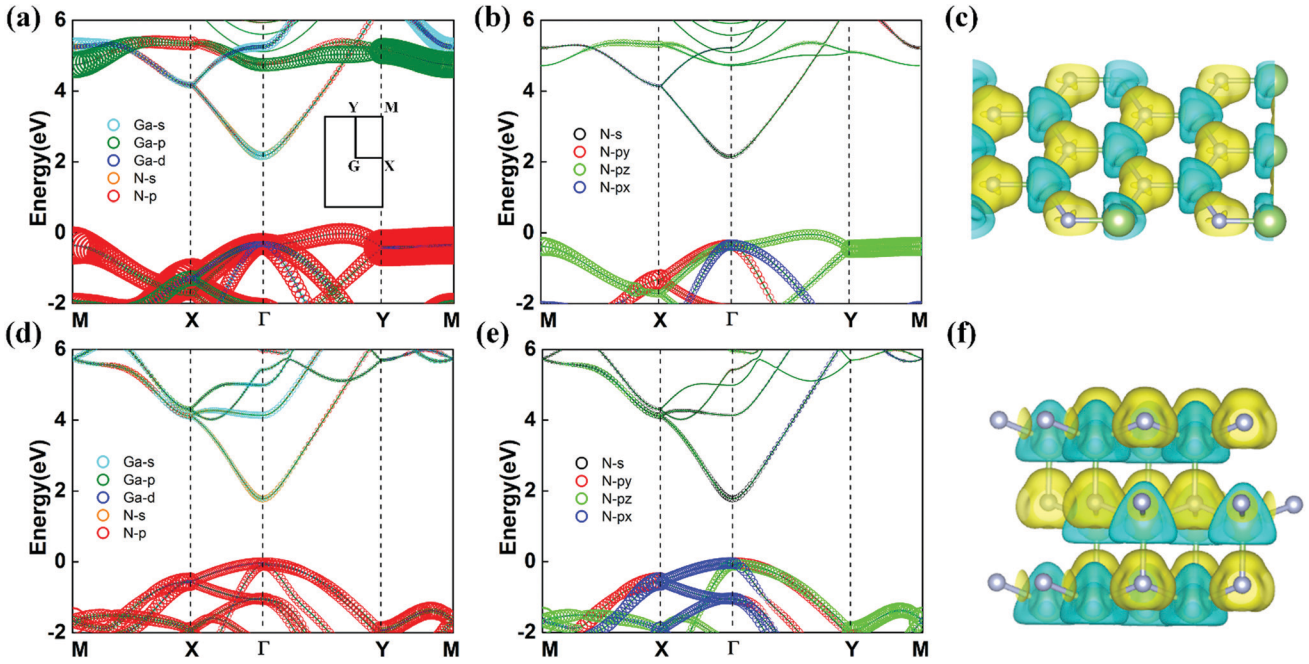

Fig. 2 Orbital projected electronic structure for (a) monolayer GaN, (b) N atom in monolayer GaN, (d) bulk GaN, and (e) N atom in bulk GaN. The charge density difference for (c) monolayer GaN and (f) bulk GaN. The isosurface is at 0.008 e Å^{-3}.

sublayer1 and inner sublayer2 as shown in Fig. 1(c). Different from the optimized *m*-plane monolayer GaN, the bilayer m-plane GaN has a buckled hexagonal structure. Different from the bulk structure, the bilayer *m*-plane consists of only two surface layers with reduced buckling. From the orbital projected electronic structure in Fig. 3(a) and (b), we can see that the main contribution to the VBM still comes from the N atom as in the monolayer GaN. However, because of the buckling, both the N atoms from the outer sublayer and the inner sublayer have significant contributions. Due to the relative locations of the two sublayers and the interaction from the two surfaces, the valence energy shows a peak not only along the *Γ*–*Y* direction, but also along the *Γ*–X direction as shown in Fig. 3(a). Specifically, the surface layer is more planar like with sp^2 hybridization while it also has some contributions from the interaction of the two surfaces. The p_z orbitals from the N atoms still contribute the most to the VBM. For bilayer *m*-plane GaN, the surface has lower coordination and is buckled, with a bandgap of 1.66 eV.

3.2.3 Band evolution with the layer numbers. Fig. 4 shows the band structures of 3ML, 4ML and 12ML GaN. The CBM locates at the *Γ* point in all the cases while the VBM shifts from the point between *Γ* and *Y* to the *Γ* point with increasing layer number. The detailed information of the band gap change with the layer number is summarized in Table 1. The lattice constant decreases with the layer number, indicating an increase of atom interaction, which will enlarge the band gap. The shortest bond length is at the surface for all the cases indicating that the surface effects could not be ignored. From the orbital projected electronic structure of Fig. 4(d)–(f), we can see that the contribution to the VBM from the surface p_z orbital of N_1 is still large, which is consistent with the large bond order of N1–Ga1. As discussed above, the planar structure has an indirect bandgap while the bandgap is direct for buckled bulk structure. The bandgap magnitude and types are mainly attributed to the lattice constant and the buckling respectively. In multilayer GaN, the surface layer has low coordination number as the monolayer does while the internal structure has the same

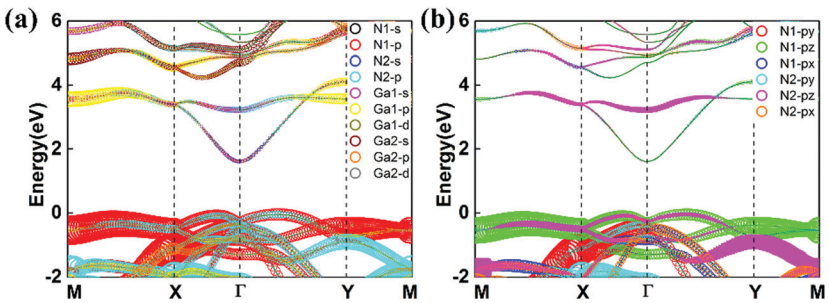

Fig. 3 Orbital projected electronic structure for (a) bilayer *m*-plane GaN and (b) N atoms in bilayer *m*-plane GaN.

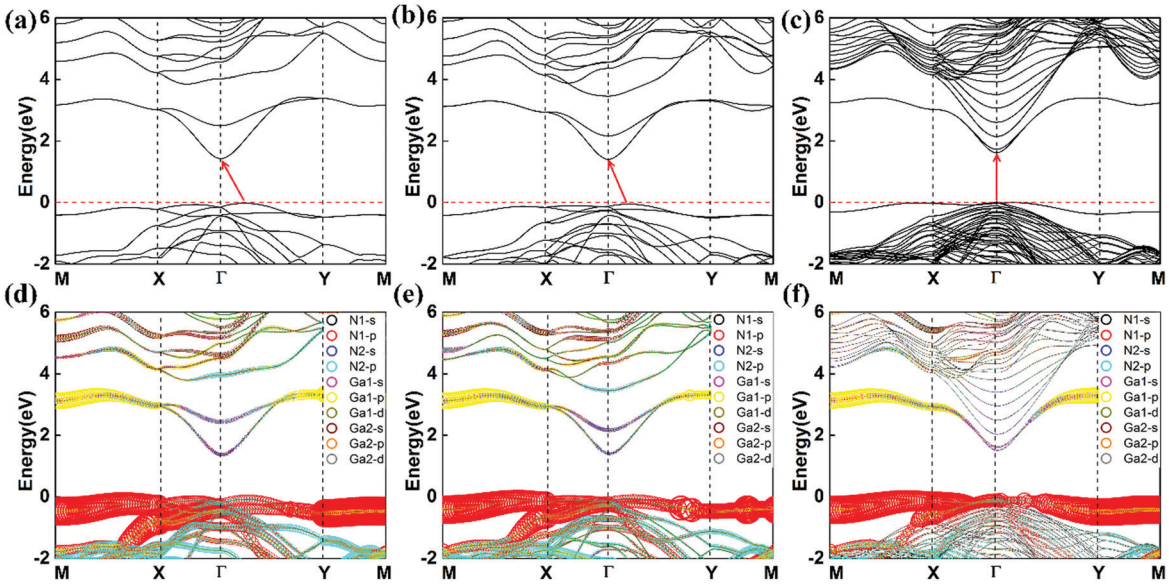

Fig. 4 Electronic structure for *m*-plane GaN at (a) 3ML, (b) 4ML, (c) 12ML and orbital projected electronic structure at (d) 3ML, (e) 4ML and (f) 12ML.

coordination number as the bulk does. The surface layer buckling due to the missing bond increases with the layer number as reflected in the bond angles ΘN_1–Ga_2–N_1 and ΘN_2–Ga_1–N_2 in Table 1. At a layer number of 12, the bandgap changes from indirect to direct. Our results at layer number larger than 12 could be compared with the previous research on the *m*-plane surface.[17] The surface N–p orbitals contribute to the VBM while the surface Ga–s orbitals locate at the CBM. From the previous experiment[16] and DFT calculation,[17,18] we can also conclude that the bandgap is mainly determined by the bulk state and tuned by the surface state. The bandgap variation with layer number in our work is consistent with these statements. The lattice constant and the surface buckling decrease while the surface bond length increases slowly with layer number, inducing a slow decrease of the bandgap. Different from bulk GaN, the surface contribution could not be ignored even at large layer number. The bandgap is still much smaller than the bulk value even at layer number 14.

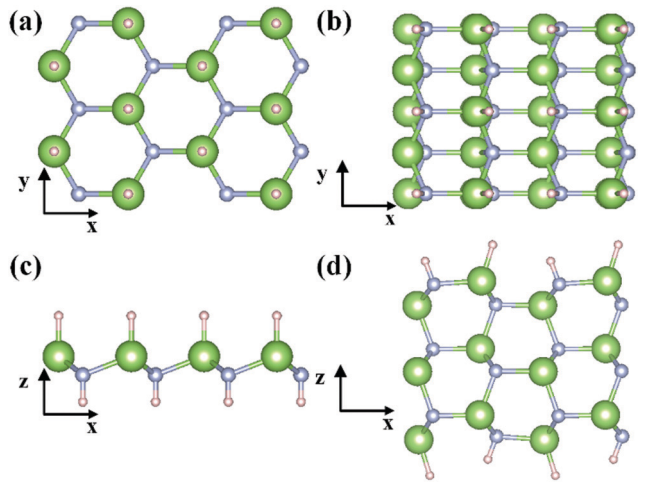

Fig. 5 Structures of surface hydrogenated monolayer *m*-plane GaN and trilayer *m*-plane GaN. Green: Ga; grey: N; pink: H.

3.3 Surface modification of *m*-plane GaN

As discussed above, because of the covalent bonding between Ga and N atoms, the multilayer GaN prefers a buckled structure. For the bulk structure, the bandgap is direct while for 2D structures with a few atomic layers, the missing bonds of the surface layer play a leading role in the indirect bandgap. It is well-known that for photonic applications, a direct bandgap is highly desirable. Here, we adopt hydrogenation and fluorination that have been proved greatly influential to the physical and chemical properties of GaN[31,32] to modify the surface of multilayer *m*-plane GaN. The optimized structures of hydrogenated monolayer and multilayer *m*-plane GaN are displayed in Fig. 5. Only the structure of trilayers is displayed as a representative of multilayers. Note that there are three possibilities for surface modification for monolayer. We have tested all three ways and focus on one commonly used structure as shown in Fig. 5(c). Detailed modification methods and phonon dispersions are given in the ESI† (see Fig. S4 and S5). With the modification of hydrogen atoms, the monolayer turns to a buckled structure. Each H atom lies on the top of Ga/N, reforming a tetrahedral unit as the bulk does. The bond angle of N_1–Ga_2–N_1 changes to 107.7°, which is close to 109.7° in bulk GaN,[19] and the Ga–N bond is extended from 1.85 Å to 1.99 Å which is closer to the bond length of bulk, 1.96 Å. Similarly, for the trilayers, the H atoms are also located above Ga/N to form a tetrahedral unit with other Ga and N atoms. The bond angles of N_1–Ga_1–N_2 and N_2–Ga_1–N_2 are 109.2° and 108.0° respectively, that is, closer to the bulk than the unmodified GaN (see Table 1 for more details). In general, *m*-plane GaN evolves to a more bulk-like structure after modification. The structure of fluorinated GaN is similar to

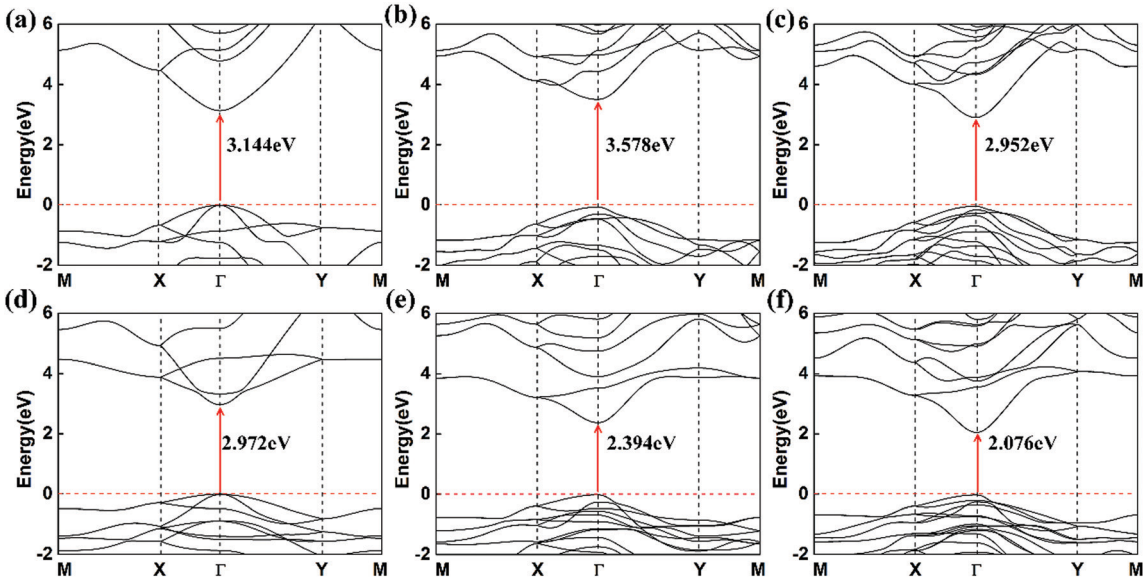

Fig. 6 Band structures of hydrogenated and fluorinated *m*-plane GaN. (a)–(c) 1ML, 2ML, 3ML hydrogenated *m*-plane GaN respectively; (d)–(f) 1ML, 2ML, 3ML fluorinated *m*-plane GaN respectively.

the hydrogenated one. After modification, the lattice constant reduced from 3.24 Å to 3.20 Å and 3.22 Å for hydrogenation and fluorination respectively.

The band structures of a few layers of hydrogenated and fluorinated *m*-plane GaN are presented in Fig. 6. It is obvious that both hydrogenation and fluorination have significantly shifted the position of the VBM compared with the unmodified one. All the VBM locate at the Γ point under modification, leading to a direct bandgap for both monolayer and multilayer *m*-plane GaN. The change of the bandgap type comes from the saturation of the surface dangling bond, resulting in a more bulk-like structure. Moreover, the introduction of hydrogen and fluorine has increased the bandgaps as noted in Fig. 6. Compared with fluorination, hydrogenation works better in enlarging the bandgaps. For example, the bandgap of unmodified trilayer *m*-plane GaN is 1.455 eV. The bandgap of hydrogenated trilayer *m*-plane GaN is 2.952 eV, that is, about two times larger than the unmodified one. The bandgap of fluorinated trilayers is 2.076 eV, indicating that the broadening effect of fluorination is less than that of hydrogenation. The enlarged bandgap comes from the decreased interactions between Ga and N atoms due to the changes of the bond length and lattice constant after chemical modifications.

4. Conclusions

The structural and electronic properties of multilayer *m*-plane GaN are investigated. It is found that the covalent bonds play an essential role in these properties. Specifically, for the monolayer, the missing bonds induce sp^2 hybridization, resulting in a planar hexagonal structure with indirect bandgap; this result appears to be general for monolayer GaN, no matter what the direction of the cutting plane from the bulk is. Bilayer GaN has two surface planes with a 3 coordinated outer sublayer and 4 coordinated inner sublayer. This buckled structure also has indirect bandgap with the main contribution of the VBM from p_z orbitals of both the outer and inner subsurface layer N atoms. Starting from the trilayer, the multilayer *m*-plane GaN consists of the surface layers and the bulk-like middle layers. With the increase of layer number, the lattice constant decreases and the surface layer buckling increases, indicating the increase of the atom interaction and a more bulk-like structure. At a layer number of 12, the bandgap changes from an indirect to direct one. The planar hexagonal monolayer structure has the largest bandgap of 2.18 eV. The bandgap of bilayer *m*-plane GaN is 1.66 eV, which is much smaller than that of the monolayer. From 3ML, the band gap increases with the layer number. Hydrogenation and fluorination provide effective ways to tune the bandgap of few-layer GaN from indirect to direct by saturating the surface dangling bonds. The enlargement of the bandgap width by hydrogenation is much larger than that by fluorination.

Conflicts of interest

There are no conflicts to declare.

Acknowledgements

D. X. acknowledges support from the National Natural Science Foundation of China (No. 51806072). J. M. acknowledges support from the National Natural Science Foundation of China (No. 11804229). X. L. acknowledges support from the Ministry of Science and Technology of the People's Republic of China (No. 2017YFE0100600). The computation was completed using the Tianhe II supercomputer in the National Supercomputing Center at Guangzhou.

Notes and references

1 X. R. Cai, Y. Y. Ren, M. H. Wu, D. W. Xu and X. B. Luo, *Nanoscale*, 2020, **12**, 167–172.
2 K. S. Novoselov, A. K. Geim, S. V. Morozov, D. Jiang, Y. Zhang, S. V. Dubonos, I. V. Grigorieva and A. A. Firsov, *Science*, 2004, **306**, 666–669.
3 Q. H. Wang, K. Kalantar-Zadeh, A. Kis, J. N. Coleman and M. S. Strano, *Nat. Nanotechnol.*, 2012, **7**, 699–712.
4 K. Momma and F. Izumi, *J. Appl. Crystallogr.*, 2011, **44**, 1272–1276.
5 N. Zhou, R. Yang and T. Zhai, *Mater. Today Nano*, 2019, **8**, 100051.
6 Y. Guo, K. Xu, C. Wu, J. Zhao and Y. Xie, *Chem. Soc. Rev.*, 2015, **44**, 637–646.
7 J. T. Robinson, J. S. Burgess, C. E. Junkermeier, S. C. Badescu, T. L. Reinecke, F. K. Perkins, M. K. Zalalutdniov, J. W. Baldwin, J. C. Culbertson, P. E. Sheehan and E. S. Snow, *Nano Lett.*, 2010, **10**, 3001–3005.
8 R. R. Nair, W. C. Ren, R. Jalil, I. Riaz, V. G. Kravets, L. Britnell, P. Blake, F. Schedin, A. S. Mayorov, S. J. Yuan, M. I. Katsnelson, H. M. Cheng, W. Strupinski, L. G. Bulusheva, A. V. Okotrub, I. V. Grigorieva, A. N. Grigorenko, K. S. Novoselov and A. K. Geim, *Small*, 2010, **6**, 2877–2884.
9 D. C. Elias, R. R. Nair, T. M. G. Mohiuddin, S. V. Morozov, P. Blake, M. P. Halsall, A. C. Ferrari, D. W. Boukhvalov, M. I. Katsnelson, A. K. Geim and K. S. Novoselov, *Science*, 2009, **323**, 610–613.
10 J. O. Sofo, A. S. Chaudhari and G. D. Barber, *Phys. Rev. B*, 2007, **75**, 153401.
11 S. P. Denbaars, D. Feezell, K. Kelchner, S. Pimputkar, C.-C. Pan, C.-C. Yen, S. Tanaka, Y. Zhao, N. Pfaff, R. Farrell, M. Iza, S. Keller, U. Mishra, J. S. Speck and S. Nakamura, *Acta Mater.*, 2013, **61**, 945–951.
12 C. L. Freeman, F. Claeyssens, N. L. Allan and J. H. Harding, *Phys. Rev. Lett.*, 2006, **96**, 066102.
13 D. Xu, H. He, R. Pandey and S. P. Karna, *J. Phys.: Condens. Matter*, 2013, **25**, 345302.
14 A. V. Kolobov, P. Fons, J. Tominaga, B. Hyot and B. Andre, *Nano Lett.*, 2016, **16**, 4849–4856.
15 P. W. Tasker, *J. Phys. C: Solid State Phys.*, 1979, **12**, 4977–4984.
16 M. Franz, S. Appelfeller, H. Eisele, P. Ebert and M. Dahne, *Phys. Rev. B*, 2019, **99**, 6.
17 M. Landmann, E. Rauls, W. G. Schmidt, M. D. Neumann, E. Speiser and N. Esser, *Phys. Rev. B: Condens. Matter Mater. Phys.*, 2015, **91**, 8.
18 V. M. Bermudez, *Surf. Sci. Rep.*, 2017, **72**, 147–315.
19 A. Onen, D. Kecik, E. Durgun and S. Ciraci, *Phys. Rev. B*, 2016, **93**, 085431.
20 Z. Z. Qin, G. Z. Qin, X. Zuo, Z. H. Xiong and M. Hu, *Nanoscale*, 2017, **9**, 4295–4309.
21 G. Kresse and J. Furthmuller, *Phys. Rev. B: Condens. Matter Mater. Phys.*, 1996, **54**, 11169–11186.
22 G. Kresse and J. Furthmuller, *Comput. Mater. Sci.*, 1996, **6**, 15–50.
23 J. P. Perdew, K. Burke and M. Ernzerhof, *Phys. Rev. Lett.*, 1996, **77**, 3865–3868.
24 S. Grimme, J. Antony, S. Ehrlich and H. Krieg, *J. Chem. Phys.*, 2010, **132**, 19.
25 A. Togo, F. Oba and I. Tanaka, *Phys. Rev. B: Condens. Matter Mater. Phys.*, 2008, **78**, 9.
26 T. A. Manz, *RSC Adv.*, 2017, **7**, 45552–45581.
27 N. G. Limas and T. A. Manz, *RSC Adv.*, 2018, **8**, 2678–2707.
28 D. W. Xu, P. Zapol, G. B. Stephenson and C. Thompson, *J. Chem. Phys.*, 2017, **146**, 12.
29 J. E. Northrup and J. Neugebauer, *Phys. Rev. B*, 1996, **53**, R10477–R10480.
30 N. X. W. Wang, J. C. Liu, G. Tang and W. T. Geng, 2020, arXiv:1908.08269v5.
31 H. Shu, X. Niu, X. Ding and Y. Wang, *Appl. Surf. Sci.*, 2019, **479**, 475–481.
32 Y. W. Mu, *J. Phys. Chem. C*, 2015, **119**, 20911–20916.